High-Resolution Microwave Studies of Ring-Structured Complexes between Trifluoroacetic Acid and Water

Bin Ouyang, Tony G. Starkey, and Brian J. Howard*

Physical and Theoretical Chemistry Laboratory, South Parks Road, University of Oxford, Oxford OX1 3QZ, United Kingdom

Received: February 9, 2007; In Final Form: May 1, 2007

The rotational spectra of the complexes between one trifluoroacetic acid molecule and up to three water molecules have been recorded using a pulsed nozzle Fourier transform microwave spectrometer. The unambiguous assignments of them are made on the basis of the agreement between the experimentally determined rotational constants and the theoretical predictions from ab initio calculations using MP2/6-311++G(2df,2pd). All the complexes exhibit hydrogen-bonded ring structures. The fine splittings observed in some of the *a*-type transitions of the trifluoroacetic acid−H_2O dimer were analyzed in terms of the likely tunneling motions of the hydrogens in the H_2O molecule. Further calculations of the equilibrium constants for these three hydrated complexes of trifluoroacetic acid were also made to evaluate their fractions against the trifluoroacetic acid monomer in the atmosphere.

1. Introduction

Complexation of acids with water has been a long intriguing topic subject to both experimental and theoretical studies. The interaction occurs via formation of a hydrogen bond with acid as the hydrogen donor and the water oxygen as the acceptor. If an electronegative center exists in the acid, another weaker hydrogen bond may be formed with this center as the hydrogen acceptor and the water as the hydrogen donor. Formation of two hydrogen bonds therefore constructs a ring-like structure in the 1:1 acid−water complex. Microwave spectroscopy studies of the 1:1 complexes of nitric acid,[1] sulfuric acid,[2] or formic acid[3] with water have confirmed this structural feature.

These 1:1 complexes between acid and water can grow by incorporation of more water molecules. Although ab initio calculations can easily predict the complexation of acid with as many as seven water molecules,[4−6] direct experimental observations of different orders of these complexes have always fallen behind the theoretical calculations. One of the few successful attempts was made by Priem et al.[3] who have observed the microwave emissions from the 1:2 formic acid and water complexes. A nearly planar eight-membered hydrogen-bonded ring was formed between the formic acid and two water molecules. The three experimentally determined principal rotational constants of this complex coincided well with those of global minimal conformation suggested by ab initio calculations. Kisiel and co-workers[7,8] have reported the rotational spectra of two other 1:2 complexes of the acids HCl and HBr with water, which were also found to exhibit ring structure.

Nitric acid complexes with more than one water molecule have also been observed in the matrix-isolation Fourier transform infrared spectroscopy study of McCurdy et al.[4] and the reflection−absorption infrared spectroscopy study of Escribano et al.[9] The shifts of some of the infrared absorption bands were used in these IR studies to determine the degree of the complexation of nitric acid with water.

In the atmosphere where both acid and water vapor are ubiquitous, collisions between the acid and water molecules are numerous. The large binding energy for acid−water complex compared to other possible Van der Waals complexes will favor the production of the complex. The equilibrium constants for acid−water complexes are normally several orders of magnitude higher than those for the much more weakly bonded Van der Waals complexes, e.g., the O_2−H_2O or O_3−H_2O, in the atmosphere.[10]

Trifluoroacetic acid (TFA) is one of the most abundant haloacetic acid in the environment.[11] It arises mainly from the atmospheric oxidation process of the hydrochlorofluorocarbons, e.g., HCFC-123, HCFC-124, and HCFC-134a.[12] It is inert with respect to reaction with OH radicals,[13,14] and the main loss pathway of it from the atmosphere is wet deposition.[15] The complexation of this acid with several water molecules is thus of fundamental importance in understanding its removal process in the gas phase.

In this paper, the complexes between trifluoroacetic acid and water have been studied by means of pulsed nozzle Fourier transform microwave spectroscopy. Ab initio calculations were used to predict the geometry and the three principal rotational constants of different orders of complexes between TFA and H_2O. Assignments of the observed microwave emission lines to different complexes were made with the aid of ab initio rotational constants. The hydrogen-bonded complexes of one TFA molecule with one, two, and three H_2O molecules, denoted as TFA−H_2O, TFA−$(H_2O)_2$, and TFA−$(H_2O)_3$, have been identified, all unequivocally pointing to hydrogen-bonded closed-ring structures.

Small splittings due to the tunneling motions in the TFA−(H_2O) complex were observed and analyzed. Additionally, partition functions of TFA and water monomer and the three hydrogen-bonded complexes between them were calculated to derive the equilibrium constants of these complexes. It is found that greater than 8% of the TFA monomer will bind with H_2O to give the TFA−(H_2O) dimer under moderate atmospheric conditions of the lower troposphere.

* Author to whom correspondence should be addressed. Fax: +44 1865 275410. E-mail: brian.howard@chem.ox.ac.uk.

10.1021/jp071130y CCC: $37.00
Published on Web 06/23/2007

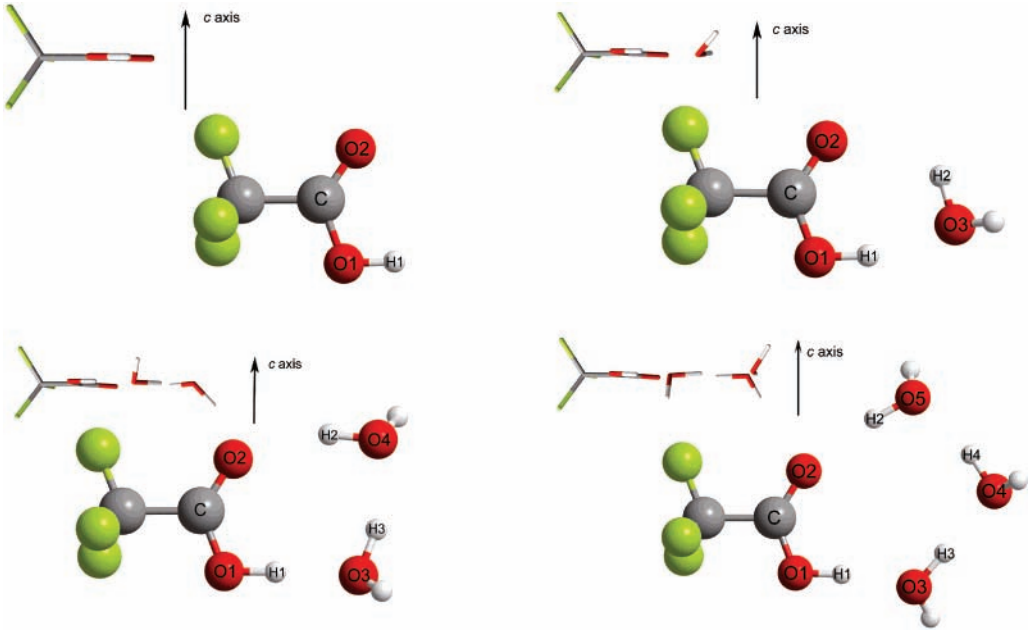

Figure 1. Geometries of the global minimal conformations of TFA, TFA−(H_2O), TFA−$(H_2O)_2$, and TFA−$(H_2O)_3$. The equatorial pictures of the TFA monomer and its complexes are shown for each at the upper left as well.

TABLE 1: Experimental Rotational Constants and Centrifugal Distortion Constants[a]

parameter	TFA	TFA−(H_2O)	TFA−$(H_2O)_2$	TFA−$(H_2O)_3$
A/MHz	3865.13430 (89)[b]	3835.107 (76)	2533.7133 (189)	1733.3501 (150)
B/MHz	2498.79448 (56)	1082.58147 (81)	718.45639 (36)	493.41249 (41)
C/MHz	2075.20197 (63)	993.78411 (77)	622.50323 (32)	414.751971 (305)
P_c[c]/uÅ^2	44.7350	45.0321	45.5175	48.6525
D_J/kHz	0.9660 (217)	0.18629 (231)	0.06942 (52)	0.13473
D_K/kHz	0.466 (61)	N/A	N/A	N/A
D_{JK}/kHz	−0.938 (62)	0.7925 (150)	0.5264 (68)	1.1215
d_1/kHz	−0.0483 (69)	−0.0126 (42)	−0.00581 (72)	−0.03073
d_2/kHz	0.3471 (51)	0.01963 (162)	0.01151 (44)	0.02785
N[d]	33	39	61	45
σ_{rms}[e]/kHz	1.54	1.02	1.64	21.51

[a] Note that D_K values are not determinable for the complexes from the current data. [b] Values in parentheses are one standard deviation of the fitted value in units of the last digit quoted. [c] Planar moment of inertia, as calculated from $P_c = (I_a + I_b - I_c)/2 = \sum_i m_i c_i^2$. The conversion factor between moment of inertia *I* and rotational constants is taken as 505379 MHz·uÅ^2. [d] Number of lines included in fitting. [e] Root-mean-square of the errors.

2. Experimental Section

All experiments were performed using a pulsed nozzle Fourier transform microwave spectrometer whose details have been presented before.[16] An outline of the spectrometer is briefly summarized below.

Microwave radiation pulses of 1 μs are introduced into a Fabry−Perot cavity by an antenna to rotationally excite the molecules. The cavity is composed of two confocal aluminum mirrors with a radius of curvature of 50 cm. The distance between the two mirrors is roughly 60 cm and can be tuned to support microwaves of different frequencies. The cavity is evacuated by an oil diffusion pump to maintain a pressure below 10^{-4} Torr.

A mixed solution of TFA and H_2O was cooled with an ice bath. Helium was bubbled through the solution to carry the TFA and H_2O vapor and to drive the supersonic expansions. The molar ratio of TFA to H_2O in the gas phase was approximately 5:4. The gas flow then passed through a pulsed nozzle with an 0.5 mm orifice and underwent supersonic expansion. Complexes were formed and cooled in the expansion, and were then excited by the microwave pulse. The emissions from the excited complexes were detected by the exciting antenna, mixed in two stages to a frequency centered on 2.5 MHz, digitized by a 10 MHz analog-to-digital card, and then transferred to PC for further analysis. All emission signals were split into Doppler doublets due to the coaxial setup of the supersonic expansion nozzle and the microwave antenna. The arithmetic mean frequency of the doublets was taken as the true transition frequency.

Microwave transitions were recorded in steps of 0.5 MHz in the region of 6.5−18.0 GHz. Averaging of 1000 to 10000 shots were performed to achieve acceptable signal-to-noise (S/N) ratios.

3. Results

3.1. Microwave Results and Assignments. Of the observed lines, several were removed first by assignment to the known transitions of the TFA monomer[17] and the $(H_2O)_2$.[18] The transitions of the TFA−(H_2O) and the TFA−$(H_2O)_2$ complexes with intensities similar to that of the TFA monomer were assigned with the aid of ab initio-predicted rotational constants (see section 3.2). After these assignments, 20 weaker lines remained. Fitting of these lines to the other conformations of the TFA−(H_2O) and the TFA−$(H_2O)_2$ complexes was tried, but has failed. Thus, higher-order complexes between TFA and H_2O, e.g., TFA−$(H_2O)_3$, were considered. A reasonable fit was

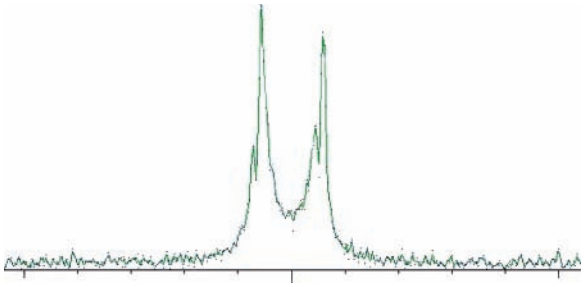

Figure 2. Small splitting observed in the $5_{1,5} \leftarrow 4_{1,4}$ transition of the TFA−H_2O dimer due to the tunneling motion of the hydrogens in water.

TABLE 2: Predicted Rotational Constants and Their Relative Deviations from the Observed Values[a]

parameter	TFA	TFA−(H_2O)	TFA−(H_2O)$_2$	TFA−(H_2O)$_3$
A/MHz	3863	3828 (3830)[b]	2531 (2561)	1721 (1752)
B/MHz	2519	1088 (1106)	718 (730)	490 (500)
C/MHz	2083	997 (1012)	622 (633)	410 (419)
P_c[c]/uÅ^2	44.4	44.8 (44.8)	45.5 (45.6)	46.2 (46.5)
($\Delta A/A$)[d]	0.06%	0.17% (−0.13%)	−0.12% (1.07%)	−0.72% (1.10%)
($\Delta B/B$)	0.79%	0.54% (2.12%)	−0.08% (1.64%)	−0.64% (1.29%)
($\Delta C/C$)	0.39%	0.37% (1.83%)	−0.15% (1.65%)	−1.05% (0.96%)
μ_a[e]/D	1.8	3.2	3.0	1.7
μ_b/D	1.5	0.2	0.2	0.1
μ_c/D	0.0	1.2	0.0	1.1

[a] The calculations were performed on the MP2/6-311++G(2df,2pd) level. [b] Values outside parentheses are for the geometries that are fully counterpoise corrected, whereas those inside parentheses are for the geometries before counterpoise corrections. [c] Planar moment of inertia P_c. The conversion factor between moment of inertia *I* and rotational constants is taken as 505379 MHz·uÅ^2. [d] Relative deviations of ab initio rotational constants, calculated as $(A_{abinitio} - A_{obs}/A_{obs}) \times 100\%$. [e] Dipole moment from ab initio based on Hartree−Fock density.

TABLE 3: Bond Lengths (Å) and Binding Energies (cm^{-1})[a] of the Global Minimal Conformations of the TFA Monomer and its Complexes from ab Initio Calculations on the MP2/6-311++G(2df,2pd) Level

parameter	TFA	TFA−(H_2O)	TFA−(H_2O)$_2$	TFA−(H_2O)$_3$
Bond Length within the TFA Fragment				
O1−H1	0.968	0.988	1.003	1.006
C−O1	1.336	1.319	1.308	1.305
C−O2	1.200	1.208	1.212	1.211
Intermolecular Hydrogen Bond Length between TFA And H_2O				
H1−O3	−	1.746	1.625	1.601
H2−O2	−	2.235	1.933	1.902
H3−O4	−	−	1.791	1.737
H4−O5	−	−	−	1.792
Binding Energies				
D_e	−	3501	7198	10075

[a] Fully counterpoise corrections of geometries made. The binding energies are free from BSSE, while no zero-point vibrational energy (ZPVE) corrections are made.

achieved with TFA−(H_2O)$_3$, which confirmed the existence of this large complex composed of four molecules in the supersonic expansion. With the fitted *A*, *B*, and *C* rotational constants from these 20 weak lines of TFA−(H_2O)$_3$, the whole set of its transitions was predicted, and 25 more lines were located near the predicted frequencies when an increased number of shots were applied.

Eleven lines are still left unassigned with very low S/N. Attempts to fit them to even larger clusters, e.g., the TFA−(H_2O)$_4$, are currently being conducted.

TFA monomer and its complexes are all prolate-top molecules. Both *a*- and *b*-type transitions have been recorded for the TFA monomer, but only *a*-type ones have been recorded

TABLE 4: Summary of the Observed Splittings in TFA−(H_2O) Complex

transition	splitting ($\Delta\nu$/kHz)	$\Delta\nu/(J+1)$
	$(J+1)_{1,J+1} \leftarrow J_{1,J}$	
$4_{1,4} \leftarrow 3_{1,3}$	13.1	3.3
$5_{1,5} \leftarrow 4_{1,4}$	15.5	3.1
$6_{1,6} \leftarrow 5_{1,5}$	18.5	3.1
$7_{1,7} \leftarrow 6_{1,6}$	22.0	3.1
$8_{1,8} \leftarrow 7_{1,7}$	25.3	3.3
	$(J+1)_{1,J} \leftarrow J_{1,J-1}$	
	for all *J*, no resolved splittings	
	$(J+1)_{0,J+1} \leftarrow J_{0,J}$	
$4_{0,4} \leftarrow 3_{0,3}$	−	−
$5_{0,5} \leftarrow 4_{0,4}$	−	−
$6_{0,6} \leftarrow 5_{0,5}$	11.7	2.0
$7_{0,7} \leftarrow 6_{0,6}$	14.0	2.0
$8_{0,8} \leftarrow 7_{0,7}$	17.1	2.1

for its three complexes with H_2O. Searches for the *b*-type transitions of the complexes in a range of ±2 MHz around the predicted frequencies with 10,000 shots yielded no signals. This may be explained by the much smaller values of μ_b than μ_a (see section 3.2). The lack of the *b*-type transitions precludes an accurate determination of the *A* rotational constant. Also the centrifugal distortion constants D_K cannot be determined, since for *a*-type transitions the K_a quantum number does not change.

No *c*-type transitions were observed for either the TFA monomer or its three complexes. For the monomer, the nearly planar symmetry of TFA[17] causes the *c*-dipole moment to be almost zero and has thus accounted for the absence of the *c*-type transitions. In the cases of the complexes, although the planar symmetry has been broken and the *c*-dipole moments of the global minimal conformations are no longer zero, quick tunneling motions of the hydrogens in H_2O is thought to displace the *c*-type transition frequencies by $\pm\nu$ (where ν denotes the tunneling frequency) from the asymmetric rotor model predictions. Searches for the displaced *c*-type transitions have been conducted, but no successful assignments have as yet been achieved. The tunneling motions are discussed in section 3.3.

The transition lines of each species are listed in Supporting Information A. The fitted principal rotational constants *A*, *B*, and *C*, together with the centrifugal distortion constants D_J, D_K, D_{JK}, d_1 and d_2 in Watson's symmetric reduced Hamiltonians, are listed in Table 1.

For the TFA−H_2O dimer, small splittings have been observed due to the tunneling motions of the two hydrogens in the H_2O fragment, which is discussed in section 3.3. Two states, one with nuclear spin statistics $I = 3$ and the other with $I = 1$, have been observed. It is therefore noteworthy that the third column of Table 1 has only listed the fitted rotational constants of the state with $I = 3$. For those of the other state, only *B* and *C* need to be modified, which can be readily derived by subtracting the ΔB and ΔC (as noted in section 3.3) to those of the listed ones.

3.2. Ab Initio Results. Ab initio calculations were performed using *Gaussian 03*[19] to give estimates of the structures of the complexes. The calculations were carried out at the second-order Møller−Plesset perturbation level (MP2)[20] with the 6-311++G(2df,2pd) basis set. Core electrons were frozen in the calculations. In the first-run of geometry optimization, no counterpoise corrections were made. After convergence, the output geometries were further optimized with full counterpoise corrections[21] in order to minimize the effects of basis set superposition error (BSSE). The binding energies were calculated by subtracting the energies of the free monomers from the counterpoise corrected energy of the whole complex.

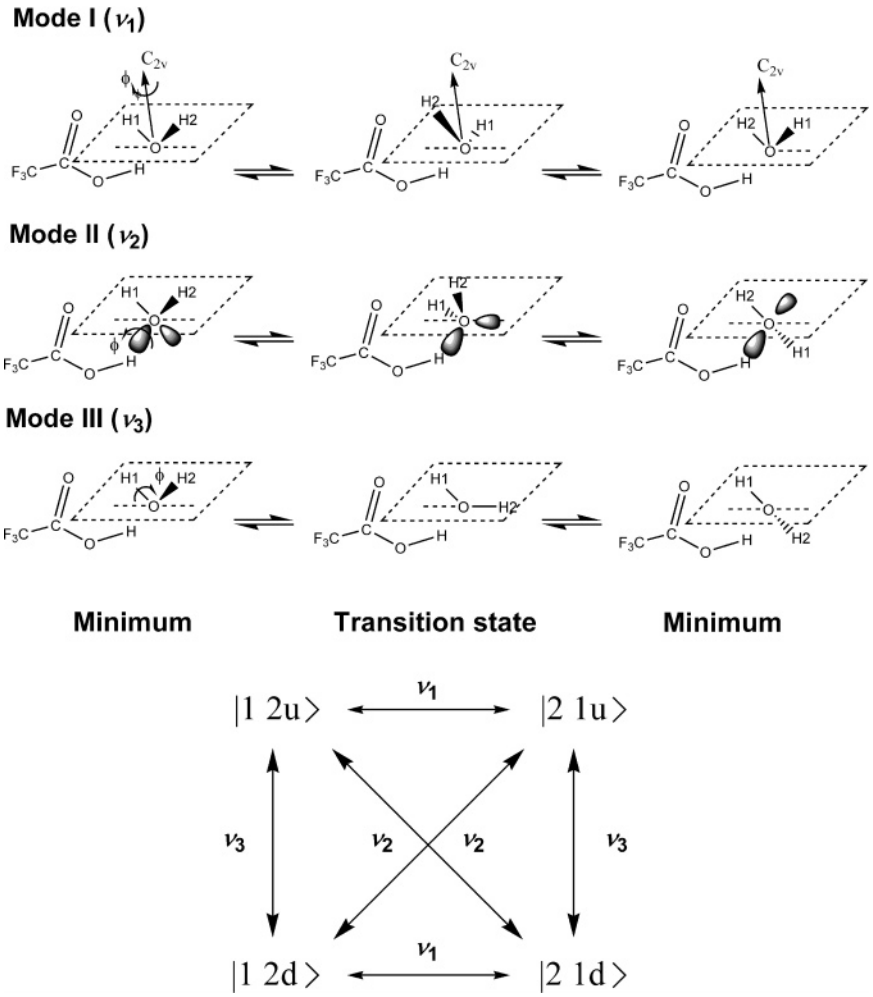

Figure 3. Three tunneling motions that connect the four minima.

The optimized geometries of the global minima of the TFA, TFA−(H_2O), TFA−(H_2O)$_2$, and TFA−(H_2O)$_3$ are shown in Figure 1. All of the hydrogen bonds in the three complexes are located in a single ring. Other conformers of these complexes with branched hydrogen bonds lie at least 1000 cm^{-1} above their global minimum. This is in agreement with the calculations of Wei et al.[5] and Aloisio et al.[22] for formic acid and H_2O complexes, and of Escribano[9] for nitric acid and H_2O complexes.

Two sets of theoretical rotational constants of the complexes, one for the geometry before the counterpoise correction and the other for that after the counterpoise correction, are included in Table 2. The good agreement with the observed values tabulated in Table 1 confirms the assignment of the microwave transitions to the three complexes shown in Figure 1.

The MP2 method with the 6-311++G(2df,2pd) basis set is a good combination for geometry predictions for these hydrogen-bonded TFA and H_2O complexes, as is evident from Table 2. The counterpoise correction has the effect of moving the monomers apart and therefore decreases the rotational constants of the complex. This modification, although minor, improves the quality of the predictions. The errors of the counterpoise corrected rotational constants are less than ±1.1% of the observations.

The relative deviations of the ab initio predicted rotational constants, as shown in Table 2, move from positive values to negative ones as the size of the complex increases, which suggests a trend from underestimating the "size" of the bulk molecule to overestimating it. The current level of theory predicts the geometry of H_2O monomer quite accurately, but for the TFA monomer, the theory seems to predict a "smaller" size. If one assumes that the geometry of the TFA monomer only changes slightly upon complexation with H_2O, then this underestimate of the monomer size will be inherited by the different complexes, which tends to make the predicted rotational constants of them larger than the observations. However, this effect is likely to be assailed by an overestimate of the intermolecular hydrogen bond length by the ab initio calculations, which makes the predicted rotational constants smaller than the observations. This trend becomes more evident when more hydrogen bonds are formed from TFA−(H_2O) to TFA−(H_2O)$_3$.

Besides the rotational constants, the planar moment of inertia, $P_c = (I_a + I_b - I_c)/2 = \sum_i m_i c_i^2$, can act as another index to test the precision of the ab initio calculations. In the case of the TFA monomer and its complexes, the magnitude of P_c reflects how many atoms and how far they are located out of the $a-b$ plane, i.e., the plane in which the carboxylic group and all of the hydrogen bonds are lying. Again start with the TFA monomer. Ab initio calculations slightly underestimate P_c of the CF_3 group, the only one that contributes to P_c of TFA.[17] When we move to TFA−(H_2O), the unbound hydrogen in H_2O sticking out of the plane (Figure 1) will make extra contribution to P_c of this complex. This extra contribution was well predicted by ab initio calculations, as the calculated ΔP_c between TFA−H_2O and TFA monomer, i.e., 0.4 uÅ^2, agreed well with the observed 0.3 uÅ^2. Reasonable agreement is also achieved in the case of TFA−(H_2O)$_2$, as the ΔP_c between this complex and

the TFA monomer from ab initio is 1.1 uÅ^2, which again compares well with the observed 0.8 uÅ^2. For the TFA$-(H_2O)_3$, however, the ΔP_c between this complex and the TFA monomer from ab initio is 1.8 uÅ^2, significantly lower than the observed 3.9 uÅ^2. This suggests that the TFA$-(H_2O)_3$ complex is *less planar* than the ab initio calculation has predicted.

Some of the covalent or hydrogen bond lengths within the hydrogen-bonded rings for the TFA monomer and the three complexes are listed in Table 3. The changes of bond lengths show a rather uniform trend on going from the TFA monomer to its higher-order complexes with water. The O1−H1 bond in the TFA fragment gradually lengthens as more H_2O molecules are added, which suggests that the hydroxylic hydrogen in the TFA is moving toward dissociation. The shortening of the C−O1 bond and lengthening of the C−O2 bond further confirm this trend. The difference between the carboxylic C−O1 and the carbonyl C−O2 bond lengths decreases from 0.136 Å in the TFA monomer to 0.111 Å in TFA$-(H_2O)$, 0.096 Å in TFA$-(H_2O)_2$, and 0.094 Å in the TFA$-(H_2O)_3$ and is expected to be 0.000 Å in CF_3COO^- anion when the TFA has fully ionized.

The intermolecular hydrogen bonds become shorter as more H_2O molecules are bound. The distance between the carbonyl oxygen O2 in the TFA fragment and its nearest bound hydrogen H2 is shortened from 2.235 Å in the TFA$-(H_2O)$ to 1.902 Å in the TFA$-(H_2O)_3$. The distance between the hydroxylic hydrogen H1 in the TFA fragment to its nearest bound oxygen O3 in H_2O is shortened from 1.746 Å to 1.601 Å. The hydrogen bond between the H_2O fragments in TFA$-(H_2O)_3$ is also found to be shorter than its counterpart in TFA$-(H_2O)_2$. The shortening of the lengths of the hydrogen bonds coincides with the increase of their bond strengths. For example, the differences in binding energies are 3700 cm^{-1} and 2870 cm^{-1}, respectively, with only one more hydrogen bond formed each time when one goes from TFA$-(H_2O)$ to TFA$-(H_2O)_2$ and then to TFA$-(H_2O)_3$. The more favorable binding sites, together with the hydrogen bond cooperativity effects,[23] account for this.

3.3. Tunneling Motions in the TFA$-(H_2O)$. Small splittings were observed in some of the *a*-type *R*-branch transitions of the TFA$-(H_2O)$ complex, as summarized in Table 4. An illustrative presentation of the splitting is shown in Figure 2. Since there are no other factors that may cause splittings, we conclude that tunneling of the two hydrogens in the H_2O fragment is responsible for the splittings. Clearly *two* tunneling states are present, each with its own set of rotational constants. To the first-order approximation, the *a*-type *R*-branch transition frequencies for an asymmetric rotor is given by:

$$\nu = \begin{cases} ((B+3C)/2)(J+1) & \text{for } (J+1)_{1,J+1} \leftarrow J_{1,J} \\ ((3B+C)/2)(J+1) & \text{for } (J+1)_{1,J} \leftarrow J_{1,J-1} \\ (B+C)(J+1) & \text{for } (J+1)_{0,J+1} \leftarrow J_{0,J} \end{cases}$$

The splittings of the different $(J+1) \leftarrow J$ transitions between the tunneling states are therefore proportional to $(\Delta B + 3\Delta C)/2$, $(3\Delta B + \Delta C)/2$, or $(\Delta B + \Delta C)$, with ΔB and ΔC denoting the difference of *B* and *C* between the two tunneling states. By dividing the observed splittings with $(J+1)$, we derive $(\Delta B + 3\Delta C)/2 = 3.2$ kHz and $(\Delta B + \Delta C) = 2.0$ kHz, as shown in Table 4. This gives $\Delta B = -0.2$ kHz and $\Delta C = 2.2$ kHz. Again no information of ΔA can be acquired because of the lack of *b*- and *c*-type transitions. Note that $(3\Delta B + \Delta C)/2$, the constant controlling the splittings of the $(J+1)_{1,J} \leftarrow J_{1,J-1}$ is 0.8 kHz, only one-third or one-quarter of those controlling the other two splittings. It is therefore not surprising that for this transition the splitting is not clearly resolved as the other two. The question follows as what are the two tunneling states we have observed?

To facilitate analysis, we can denote the conformations with H1 bound in the plane and H2 lying above or below the plane as $|12u\rangle$ and $|12d\rangle$, respectively. Similarly $|21u\rangle$ and $|21d\rangle$ can represent the other two conformations with H2 bound in the plane and H1 lying above or below the plane. The interconversion of these four conformations requires the tunneling of the two hydrogens in the H_2O fragment, by undergoing "hindered rotation" about the C_2 axis of H_2O (Mode I), about the lone pair of the O atom (Mode II) or about the in-plane O−H bond (Mode III). These three motions effectively connect the four minimal conformations, as shown in Figure 3. ν_1, ν_2 and ν_3 are used to denote the tunneling frequencies associated with the three tunneling modes.

Since the TFA$-(H_2O)$ complex is non-rigid, it does not have a definite point group. Thus we have to consider the permutation-inversion group in order to construct the tunneling wavefunctions. The permutation and inversion group[24] in terms of the two hydrogen nuclei in H_2O is E, (12), E*, (12)*. If we start with the conformation $|12u\rangle$, then these four operations in the group will generate the conformations $|12u\rangle$, $|21u\rangle$, $|12d\rangle$ and $|21d\rangle$, respectively. It is noteworthy that the label such as $|12u\rangle$ indicates the internal vibronic wavefunction for the corresponding conformation.

The character table for this permutation-inversion group is shown in Table A-5 in ref 24. With the help of the character table, the tunneling wavefunctions of the four states can be constructed as:

$$\Phi_1 = \frac{1}{2}\{|12u\rangle + |21u\rangle + |12d\rangle + |21d\rangle\}$$

$$\Phi_2 = \frac{1}{2}\{|12u\rangle + |21u\rangle - |12d\rangle - |21d\rangle\}$$

$$\Phi_3 = \frac{1}{2}\{|12u\rangle - |21u\rangle + |12d\rangle - |21d\rangle\}$$

$$\Phi_4 = \frac{1}{2}\{|12u\rangle - |21u\rangle - |12d\rangle + |21d\rangle\}$$

The energy of the four tunneling states can be derived by calculating the matrix element $\langle\Phi_i|\mathscr{H}|\Phi_i\rangle$. For example, the energy of state 1 is:

$$\langle\Phi_1|\mathscr{H}|\Phi_1\rangle = \frac{1}{4}\{[\langle 12u| + \langle 21u| + \langle 12d| + \langle 21d|]\mathscr{H}[|12u\rangle + |21u\rangle + |12d\rangle + |21d\rangle]\}$$
$$= E_0 - \frac{h\nu_1}{2} - \frac{h\nu_2}{2} - \frac{h\nu_3}{2}$$

by noting that:

$$\langle 12u|\mathscr{H}|12u\rangle = \langle 21u|\mathscr{H}|21u\rangle = \langle 12d|\mathscr{H}|12d\rangle = \langle 21d|\mathscr{H}|21d\rangle = E_0$$

$$\langle 12u|\mathscr{H}|21u\rangle = \langle 21u|\mathscr{H}|12u\rangle = \langle 12d|\mathscr{H}|21d\rangle = \langle 21d|\mathscr{H}|21d\rangle = -\frac{h\nu_1}{2}$$

$$\langle 12u|\mathscr{H}|21d\rangle = \langle 21d|\mathscr{H}|12u\rangle = \langle 12d|\mathscr{H}|21u\rangle = \langle 21u|\mathscr{H}|12d\rangle = -\frac{h\nu_2}{2}$$

$$\langle 12u|\mathscr{H}|12d\rangle = \langle 12d|\mathscr{H}|12u\rangle = \langle 21u|\mathscr{H}|21d\rangle = \langle 21d|\mathscr{H}|21u\rangle = -\frac{h\nu_3}{2}$$

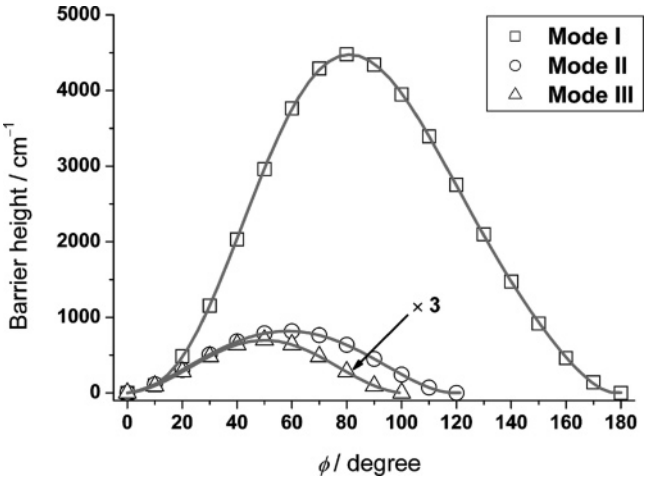

Figure 4. Barrier for the three tunneling modes. The barrier for Mode III has been multiplied by a factor of 3 to make it observable.

in which E_0 is all the other energies other than the tunneling one, while ν_1, ν_2, and ν_3 are the tunneling frequencies of the three tunneling modes shown in Figure 3. The energy of the other three states can be derived in a similar way. The relative energies of the four states, after discarding E_0, are therefore:

$$E_1/h = -\frac{\nu_1}{2} - \frac{\nu_2}{2} - \frac{\nu_3}{2}$$

$$E_2/h = -\frac{\nu_1}{2} + \frac{\nu_2}{2} + \frac{\nu_3}{2}$$

$$E_3/h = +\frac{\nu_1}{2} + \frac{\nu_2}{2} - \frac{\nu_3}{2}$$

$$E_4/h = +\frac{\nu_1}{2} - \frac{\nu_2}{2} + \frac{\nu_3}{2}$$

In terms of energy sequence, state 1 no doubt lies on the lowest level, whereas the order of the other three depends on the relative magnitude of the tunneling frequencies ν_1, ν_2, and ν_3. According to the following equation proposed by Dennison and Uhlenbeck,[25] the magnitude of the tunneling frequency ν is given by:

$$\nu = \frac{\nu_0}{\pi} \times \exp\left(-\frac{2}{h}\right) \int_0^{x_0} [2\mu(V - W)]^{1/2}\, dx$$

in which ν is the tunneling frequency, ν_0 is the frequency of the related vibration, x_0 is a half of the tunneling distance, μ is the reduced mass of the tunneling motion, V is the barrier height of the tunneling motion, and W is the total vibrational energy. The potential curves $V(x)$ for the three possible tunneling motions have been scanned using MP2/6-311++G(2df,2pd). The results are shown in Figure 4. The geometries of the TFA and H_2O fragments were frozen during the scan for consideration of computer costs. It is not surprising to obtain a much higher barrier for mode I than for modes II and III since tunneling of the two hydrogens around the C_2 axis moves both the hydrogen-bonded H and the lone pair of the O atom in the H_2O fragment, and thus breaks both hydrogen bonds between TFA and H_2O.

The candidate vibrations that may help to overcome the tunneling barrier fall in the range of 140−440 cm^{-1} (calculated on HF/6-31(d) level and then scaled, see Supporting Information B). The fourth normal mode (149 cm^{-1}) can be easily identified as the one related to the tunneling mode III, whereas for the remaining two tunneling modes, a clear connection of them with

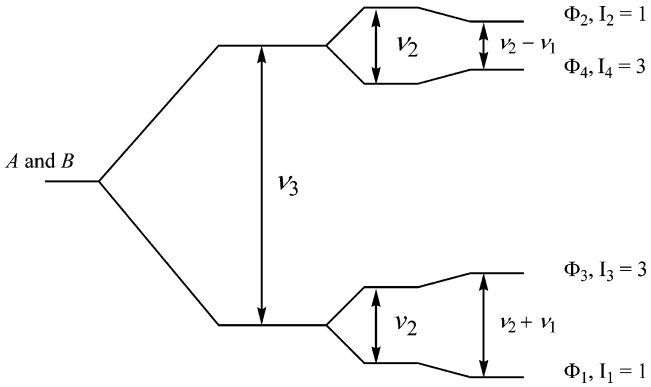

Figure 5. Energy diagram of the four tunneling states of TFA−(H_2O). *I* is the nuclear spin statistical weight of the state.

TABLE 5: Equilibrium Constants of TFA−(H_2O) and TFA−(H_2O)$_2$ at Different Temperatures with Standard Pressure $p^0 = 1$ bar

	equilibrium constant	
temp (K)	TFA−(H_2O)	TFA−(H_2O)$_2$
320	1.44	7.75×10^{-1}
310	2.20	1.83
300	3.46	4.58
290	5.64	1.23×10
280	9.52	3.52×10
270	1.67×10	1.09×10^2
260	3.07×10	3.74×10^2
250	5.94×10	1.41×10^3
240	1.21×10^2	5.95×10^3
230	2.64×10^2	2.85×10^4
220	6.20×10^4	1.58×10^5
210	1.58×10^5	1.03×10^6
200	4.41×10^3	8.18×10^6

any of the fundamental vibrations is difficult. However, since tunneling mode II has both a longer tunneling distance and a higher barrier than mode III (as shown in Figure 4), it is reasonable to conclude that the tunneling for mode II will be more difficult than mode III, and the frequency connected with this mode, i.e., ν_2 should be smaller than ν_3. By analogy, tunneling mode I with a similar tunneling distance, but a barrier height 5−8 times higher than mode II is no doubt the most difficult one, and ν_1 should be much smaller than both ν_2 and ν_3. Using the equation of Dennison and Uhlenbeck, we have qualitatively calculated ν_3 to be about 11 cm^{-1}, while both ν_1 and ν_2 are smaller than 2 cm^{-1} with $\nu_1 \ll \nu_2$.

In light of the above order of tunneling frequencies, the energy diagram of the four tunneling states can be plotted, as shown in Figure 5.

In the presence of the tunneling of the hydrogens, we also have to consider nuclear spin statistical weights. The statistical weight of a state is determined by the symmetry of the state with respect to the interchange of identical hydrogen atoms. The tunneling wavefunction will be symmetric if the character for operation (12) on the state is +1, and will be asymmetric if the character is −1. Because the hydrogen nuclei are spin half fermions, the symmetric tunneling wavefunctions can only combine with asymmetric nuclear spin functions, while the asymmetric ones can only combine with the symmetric nuclear spin functions, to make the overall wavefunction asymmetric. From this argument, we deduce the nuclear spin statistical weight of state Φ_1, Φ_2, Φ_3, and Φ_4 to be 1, 1, 3, and 3, respectively.

The intensity ratio of the two observed split transitions (see Figure 2) is approximately 1:3. This ratio, in conjunction with

the above analysis on nuclear spin statistical weights, suggests that we have actually observed two states out of the total four, with one being singlet and the other being triplet. In consideration of the strong cooling effect of the helium supersonic expansion (to ~1 K), the populations on the two upper states (~11 cm^{-1} higher than the two lower ones) must have been completely converted to the two lower ones, i.e., from Φ_2 to Φ_1 and from Φ_4 to Φ_3, which is allowed by nuclear spin selection rule. The depopulation from Φ_3 to Φ_1 is forbidden by the same selection rule. This explains why *two* states are present in the expansions.

Interestingly, similar 3:1 doublets have also been observed in the microwave spectroscopy study of a similar acid−water complex, i.e., the HNO_3-H_2O, by Canagaratna et al.[1] Moreover, they noticed that the observed tunneling was completely quenched when the out-of-plane H was substituted by D. This result is again in agreement with current analysis. When the two hydrogens are not identical, tunneling modes 1 and 2 in Figure 3 will no longer be feasible. $\nu_1 + \nu_2$ as a result will be zero, which means that the two observed tunneling states 1 and 3 will merge into a single one with no splittings observed.

The selection rules for electric dipole transitions can be determined with reference to the group theory. In summary, rotational transition selection rules for the four tunneling states are:

(1) for *a*- and *b*-type rotational transitions, $\Phi_1 \leftrightarrow \Phi_1$, $\Phi_2 \leftrightarrow \Phi_2$, $\Phi_3 \leftrightarrow \Phi_3$, and $\Phi_4 \leftrightarrow \Phi_4$ are allowed.

(2) for *c*-type rotational transitions, $\Phi_1 \leftrightarrow \Phi_2$ and $\Phi_3 \leftrightarrow \Phi_4$ are allowed.

According to the selection rules discussed above, the *c*-type transitions can only occur between different tunneling states. This will move the *c*-type transition frequencies by ,$\pm\nu$ (where ν is the tunneling frequency) from the asymmetric rotor model predictions. The operator $\hat{\mu}_c$ that connect the two states is not that of any of the four fully delocalized tunneling state whose *c*-dipole moment is obviously zero, but that of the four localized global minima whose *c*-dipole is not zero. From this point of view, the *c*-type transitions between different tunneling states are only observable if the frequency range $\nu_3 \pm \nu_2$ is covered.

3.4. Partition Functions and Equilibrium Constants. The equilibrium between the complexes and the monomers are listed in eq 1. The equilibrium constants can be calculated by deriving the partition functions of each species.[26]

$$\begin{aligned} TFA + H_2O &\rightleftharpoons TFA-(H_2O) \\ TFA + 2H_2O &\rightleftharpoons TFA-(H_2O)_2 \end{aligned} \quad (1)$$

The translational and rotational partition functions of the different species can be readily determined since the mass and the rotational constants of all of the species are known. For zero-point vibrational energy (ZPVE) corrections to binding energy and for the calculation of vibrational partition functions, we also need the vibrational frequencies of the monomers and complexes. The required binding energies D_e were calculated at the MP2/6-311++G(2df,2pd) level, as shown in Table 3. The calculation of vibrational frequencies were conducted at the HF/6-31G(d) level. This combination of method and basis set has been tested for a wide range of molecules by Scott and Radom[27] and has been recommended as one of the most successful combinations.

As a further test of the performance of HF/6-31G(d), we have calculated the vibrational frequencies of the TFA and H_2O monomers, scaled them by following the procedures elaborated in the work of Scott and Radom,[27] and then compared them with the experimental ones. The results were shown in Supporting Information B. Good agreement can be found between the calculated and the experimental values.

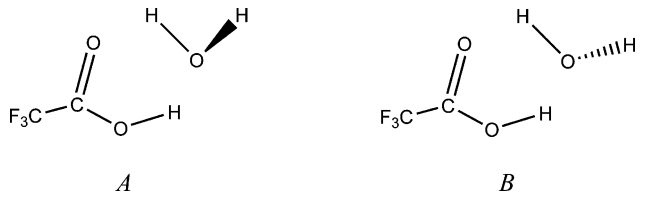

Figure 6. Two distinguishable conformations of TFA−(H_2O).

Special attention is required in determining the effect of tunneling motions on the magnitude of partition functions. Consider the TFA−(H_2O) complex as an example. If the tunneling motions were absent, we will end up with two "independent" conformations, one with the unbound hydrogen pointing "up" the plane and the other with the unbound hydrogen pointing "down", as shown in Figure 6. These two conformations have degenerate energy levels because they are the mirror images of each other, but they are also an enantiomeric pair since they cannot be interchanged by three-dimensional free rotations. The partition function of TFA−(H_2O) should therefore be multiplied by a factor of 2.

When the tunneling motions are present, the energy levels will be split and we will end up with four tunneling states with different nuclear spin statistical weights, as shown in Figure 5. The two lower states will be slightly favored by Boltzmann distribution, whereas the two upper ones will be disfavored. The equilibrium constant of the TFA−(H_2O) complex against the monomers in the presence of tunneling can be calculated using eq 2.

$$K_{p,TFA-(H_2O)} = \sum_n \left(q_n^0 \times e^{D_n/k_T} \times \frac{I_n}{4} \times (N_A)^2 \right) / (q_{TFA}^0 \times (q_{H_2O}^0)^2) \quad (2)$$

where q_n, D_n, and I_n denote the overall partition function, the dissociation energy, and the nuclear spin statistical weight of the *n*th tunneling state, respectively. N_A is the Avogadro constant. The 4 in the denominator is the number of nuclear spin functions for two hydrogens. $q_{1\rightarrow n}$ have been assumed to be the same as that of the global minimum conformation *A*. I_n has been derived in section 3.3. D_n is calculated with eq 3 where D_0 is the dissociation energy of the global minimum conformation *A* (or *B*).

$$\begin{aligned} D_1 &= D_0 + h\left(\frac{\nu_1 + \nu_2 + \nu_3}{2}\right) \\ D_2 &= D_0 + h\left(\frac{\nu_1 - \nu_2 - \nu_3}{2}\right) \\ D_3 &= D_0 + h\left(\frac{-\nu_1 + \nu_2 - \nu_3}{2}\right) \\ D_4 &= D_0 + h\left(\frac{-\nu_1 - \nu_2 + \nu_3}{2}\right) \end{aligned} \quad (3)$$

For TFA−(H_2O)$_2$, the number of distinguishable conformations is four, as shown in Figure 7. The energies of conformation *A*′ and *B*′ are degenerate since they are the mirror images of

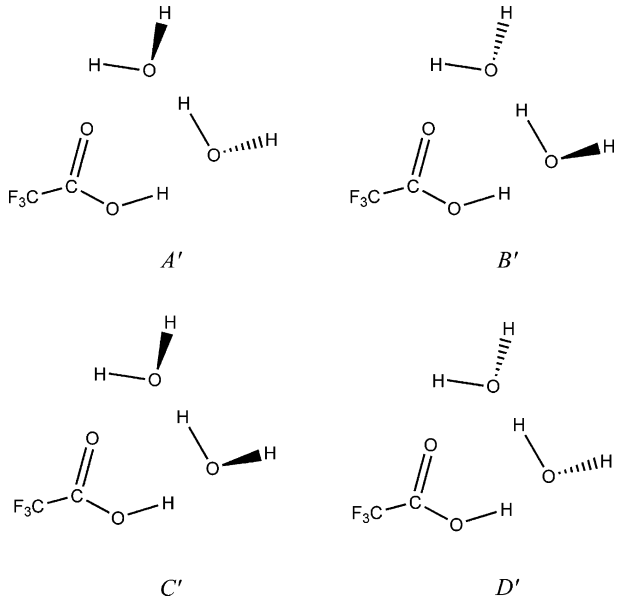

Figure 7. Four distinguishable conformations of TFA−$(H_2O)_2$.

each other. This also applies to conformation C' and D'. However, the dissociation energy difference ΔD_0 between A' and C' is about 43 cm^{-1}. The interactions between the wavefunctions of conformations A' and B' and those of conformations C' and D' are therefore assumed to be negligible since the energy degeneracy is lost. Analysis of the tunneling states and their nuclear spin statistical weights have been included in Appendix A. The energy diagram for the tunneling states in TFA−$(H_2O)_2$ is plotted in Figure 8.

The equilibrium constant of TFA−$(H_2O)_2$ against the monomers is calculated according to eq 4.

$$K_{p,\mathrm{TFA}-(\mathrm{H_2O})_2} = \sum_n \left(q_n^0 \times \mathrm{e}^{D_n/k_\mathrm{T}} \times \frac{I_n}{4} \times (N_\mathrm{A})^2 \right) / (q_\mathrm{TFA}^0 \times (q_{\mathrm{H_2O}}^0)^2) \quad (4)$$

where q_n, D_n, and I_n denote the same parameters used in eq 6. The 16 in the denominator is scaling factor to take account the number of nuclear spin functions for four hydrogens.

For TFA−$(H_2O)_2$, the hydrogens in the two H_2O molecules are required to tunnel simultaneously to yield the other degenerate conformation, e.g., from A' to B' or from C' to D'. Both the tunneling mass and the tunneling barrier will roughly double when going from TFA−(H_2O) to TFA−$(H_2O)_2$, which will lower the magnitude of tunneling frequencies exponentially. Given that even the largest tunneling frequency in TFA−(H_2O) is only about 11 cm^{-1}, it is fairly safe to conclude that the upper limit of the tunneling frequencies in TFA−$(H_2O)_2$ should not have exceeded 5 cm^{-1}. This small splitting of energy levels is of negligible influence upon the partition function of the species when the temperature range in question is between 200−320 K (typical tropospheric temperatures), which implies that:

$$D_{1\to 8} \cong D_A' = D_0$$
$$D_{9\to 16} \cong D_{C'} = D_0 - \Delta D_0 \quad (5)$$

where D_0 is the dissociation energy of the minimal conformation A' shown in Figure 7, and ΔD_0 is the dissociation energy difference between conformation A' and C', i.e. 43 cm^{-1}.

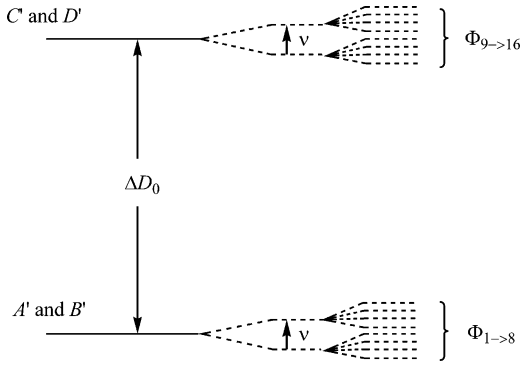

Figure 8. Energy diagram of the TFA−$(H_2O)_2$. ΔD_0 is the dissociation energy difference between the minimal conformations A' and C' shown in Figure 7. ν denotes the tunneling frequency with $\nu \ll \Delta D_0$. The dashed lines mean that the exact energy sequence of the tunneling states is not clearly resolved.

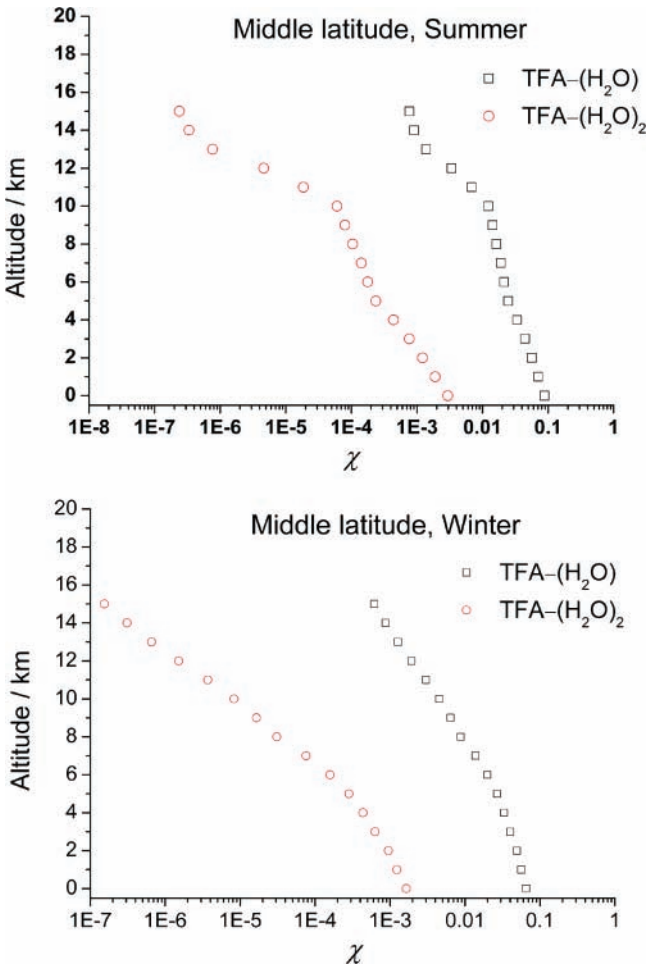

Figure 9. Ratio of the mixing pressures of the TFA complexes to that of the TFA monomer.

The calculated equilibrium constants at different temperatures are tabulated in Table 5. The ratio χ of the mixing pressures of the complexes to that of the monomer of TFA in the atmosphere can be calculated with eq 6.

$$\chi_{\mathrm{TFA}-(\mathrm{H_2O})} = \frac{p_{\mathrm{TFA}-(\mathrm{H_2O})}}{p_\mathrm{TFA}} = K_{p,\mathrm{TFA}-(\mathrm{H_2O})} \times \frac{p_{\mathrm{H_2O}}}{p^0}$$
$$\chi_{\mathrm{TFA}-(\mathrm{H_2O})_2} = \frac{p_{\mathrm{TFA}-(\mathrm{H_2O})_2}}{p_\mathrm{TFA}} = K_{p,\mathrm{TFA}-(\mathrm{H_2O})_2} \times \left(\frac{p_{\mathrm{H_2O}}}{p^0}\right)^2 \quad (6)$$

Using the equilibrium constants in Table 5 and the atmospheric mixing pressure of water vapor, it is possible to estimate χ at different altitudes. The values of the mixing pressure of water vapor and the temperature at different altitudes are taken from the work of Ellingson et al.[28] The calculated χ are shown in Figure 9.

Our current calculation shows that about 8% TFA monomer will bind with H_2O to form the TFA$-(H_2O)$ dimer in the lower troposphere (0−1 km). However, we believe that there is a large error associated with this result due to the underestimate of the binding energy, which will be discussed briefly in the next section. The fractions of even higher-order complexes, e.g., TFA$-(H_2O)_2$, are of more than 1 order of magnitude lower than the dimer. As the altitude increases, formation of the complexes will be less favored due to the sharp decrease of the concentration of H_2O vapor. This trend holds in both the summer and the winter.

4. Discussion

The experimentally observed rotational constants of the three different orders of complexes between TFA and H_2O coincide with the ab initio predictions. All three complexes possess ring structures in which all of the hydrogen bonds are located. The ab initio results indicate that conformations with ring structures are the global minima for all three complexes.

The identification of the TFA$-(H_2O)_3$ tetramer indicates the formation of this species by collisions between the existing clusters in the expansions, which are much less frequent than those between the monomers. The formation of TFA$-(H_2O)_3$ illustrates the "sticky" nature of the H_2O molecules.

Attempts to identify even larger ring-structured complexes are currently being conducted. The formation of these complexes is thermodynamically favored since the temperature in the supersonic expansions is as low as 1 K. However, kinetically the formation of large clusters requires the participation of smaller clusters or monomers. Given the requirement of multiple collisions, the concentration of larger clusters is likely to be less. Moreover, larger clusters have larger rotational partition functions and hence the population per level will again be less, making the observation of their spectral lines more difficult.

There are several papers available in which the equilibrium constants of the 1:1 hydrates are evaluated for different acids, e.g., hydrate of nitric acid,[29] nitrous, nitric, and pernitric acid.[30] However, the authors do not seem to have taken into account the chirality of the complexes when calculating the equilibrium constants. We believe that all of the equilibrium constants need to be multiplied by a factor of 2 in order to account for the chirality effect.

The greatest uncertainty in the determination of the equilibrium constants lies in that of the binding energy, the magnitude of which will be influenced both by the method and by the basis set applied. The current level of theory used to calculate the binding energy is MP2/6-311++G(2df,2pd), which seems to perform quite well in predicting the geometries, but is not sufficient if accurate binding energies are desired. For example, we have examined the performance of this combination on the calculation of the binding energy of $(H_2O)_2$, the value of which has been evaluated on the CCSD(T)/aug-cc-pV6Z level.[31] The CCSD(T)/aug-cc-pV6Z binding energy is 10% larger than that from MP2/6-311++G(2df,2pd), which gives some indication that the current level is not adequate for the accurate calculations of binding energies.

To check the influence of basis set choice, the binding energy of the formic acid$-(H_2O)$ dimer has been calculated with the 6-311++G(2df,2pd) and aug-cc-pVTZ basis sets, both with the MP2 method. The binding energy from the former basis set is about 200 cm^{-1} lower than that from the latter one, which serves as another example illustrating that the binding energies of the complexes may have been underestimated. Because of the large size of the system in question, it is not viable to apply either a higher correlation method or a larger basis set to calculate the binding energies.

If we assume that the true binding energy is about 10% higher than the one we calculated using MP2/6-311++G(2df,2pd) (this value was taken from that of the $(H_2O)_2$ case), the equilibrium constant of the TFA$-(H_2O)$ and TFA$-(H_2O)_2$ will correspondingly be increased by factors of 5 and 30, respectively, at $T =$ 300 K. The fractions of TFA$-(H_2O)$ and TFA$-(H_2O)_2$ at the lower troposphere in mid-latitude region are therefore 40% and 8%, respectively, of the TFA monomer. This implies that the abundance of these TFA complexes may be comparable to that of the monomer in the atmosphere. How the physical and chemical behavior of TFA and its lifetime will be affected by complexation with H_2O in the atmosphere is therefore worthy of further investigation.

Acknowledgment. The support of the EPSRC is gratefully acknowledged. B.O. expresses his thanks for the Ministry of Education of P.R. China and the British Department for Education and Skills for jointly providing the China/UK Postgraduate Scholarship to support his study at the University of Oxford.

Appendix A

Tunneling Wavefunctions of TFA$-(H_2O)_2$. The four hydrogen atoms in the two H_2O molecules can be labeled as 1, 2, 3, and 4, respectively, with 1 and 2 in the H_2O binding to the carbonyl oxygen of TFA and 3 and 4 in the H_2O binding to the carboxylic hydrogen of TFA. Accordingly, the minimal conformation A' in Figure 7 is denoted as $|1\ 2u\ 3\ 4d\rangle$. The feasible permutation and inversion operations for this conformation will be E, (12), (34), (12)(34), E^*, (12)*, (34)*, and (12)(34)*, if we assume that "hindered" rotations around the C_2 axis, the lone pair of H_2O molecule and the in-plane O−H bond of H_2O are feasible. These operations will then give us the following conformations which are all degenerate in energy with A'. Denote them as $\Phi_1 \rightarrow \Phi_8$, respectively.

$$E\text{: } |1\ 2u\ 3\ 4d\rangle \rightarrow |1\ 2u\ 3\ 4d\rangle$$

$$(12)\text{: } |1\ 2u\ 3\ 4d\rangle \rightarrow |2\ 1u\ 3\ 4d\rangle$$

$$(34)\text{: } |1\ 2u\ 3\ 4d\rangle \rightarrow |1\ 2u\ 3\ 4d\rangle$$

$$(12)(34)\text{: } |2\ 1u\ 4\ 3d\rangle \rightarrow |1\ 2u\ 3\ 4d\rangle$$

$$E^*\text{: } |1\ 2u\ 3\ 4d\rangle \rightarrow |1\ 2d\ 3\ 4u\rangle$$

$$(12)^*\text{: } |1\ 2u\ 3\ 4d\rangle \rightarrow |2\ 1d\ 3\ 4u\rangle$$

$$(34)^*\text{: } |1\ 2u\ 3\ 4d\rangle \rightarrow |1\ 2d\ 4\ 3u\rangle$$

$$(12)^*(34):\ |1\ 2u\ 3\ 4d\rangle \rightarrow |2\ 1d\ 4\ 3u\rangle$$

The character table for this group is shown as Table A-23 in ref 24.

The nuclear spin statistical weight of a specific tunneling state can be determined by examining the characters of the (12) and (34) operations of this state. Take the state Φ_2 as an example. The character of (12) is 1 and that of (34) is also 1, which means that the tunneling wavefunction is both symmetric with respect to the interchange of hydrogen 1 and 2 and is symmetric with respect to the interchange of hydrogen 3 and 4. As a result, it shall combine with the asymmetric nuclear spin wavefunction of hydrogen 1 and 2 and with the asymmetric nuclear spin wavefunction of hydrogen 3 and 4 because hydrogen is a Fermi−Dirac particle. The nuclear spin statistical weight of Φ_2 is therefore $1 \times 1 = 1$.

The eight tunneling wavefunctions for states $\Phi_1 \leftrightarrow \Phi_8$ can be constructed with the help of the character table. They are shown together with their respective spin statistical weights in eq 7

$$\Phi_1 = \frac{1}{\sqrt{8}}\{|1\ 2u\ 3\ 4d\rangle + |2\ 1u\ 3\ 4d\rangle + |1\ 2u\ 3\ 4d\rangle + |1\ 2d\ 3\ 4u\rangle + |1\ 2u\ 3\ 4d\rangle + |2\ 1d\ 3\ 4u\rangle + |1\ 2d\ 4\ 3u\rangle + |2\ 1d\ 4\ 3u\rangle\} \quad I_1 = 1$$

$$\Phi_2 = \frac{1}{\sqrt{8}}\{|1\ 2u\ 3\ 4d\rangle + |2\ 1u\ 3\ 4d\rangle + |1\ 2u\ 3\ 4d\rangle - |1\ 2d\ 3\ 4u\rangle + |1\ 2u\ 3\ 4d\rangle - |2\ 1d\ 3\ 4u\rangle - |1\ 2d\ 4\ 3u\rangle - |2\ 1d\ 4\ 3u\rangle\} \quad I_2 = 1$$

$$\Phi_3 = \frac{1}{\sqrt{8}}\{|1\ 2u\ 3\ 4d\rangle - |2\ 1u\ 3\ 4d\rangle + |1\ 2u\ 3\ 4d\rangle + |1\ 2d\ 3\ 4u\rangle - |1\ 2u\ 3\ 4d\rangle - |2\ 1d\ 3\ 4u\rangle + |1\ 2d\ 4\ 3u\rangle - |2\ 1d\ 4\ 3u\rangle\} \quad I_3 = 3$$

$$\Phi_4 = \frac{1}{\sqrt{8}}\{|1\ 2u\ 3\ 4d\rangle - |2\ 1u\ 3\ 4d\rangle - |1\ 2u\ 3\ 4d\rangle + |1\ 2d\ 3\ 4u\rangle + |1\ 2u\ 3\ 4d\rangle - |2\ 1d\ 3\ 4u\rangle - |1\ 2d\ 4\ 3u\rangle + |2\ 1d\ 4\ 3u\rangle\} \quad I_4 = 9$$

$$\Phi_5 = \frac{1}{\sqrt{8}}\{|1\ 2u\ 3\ 4d\rangle - |2\ 1u\ 3\ 4d\rangle + |1\ 2u\ 3\ 4d\rangle - |1\ 2d\ 3\ 4u\rangle - |1\ 2u\ 3\ 4d\rangle + |2\ 1d\ 3\ 4u\rangle - |1\ 2d\ 4\ 3u\rangle + |2\ 1d\ 4\ 3u\rangle\} \quad I_5 = 3$$

$$\Phi_6 = \frac{1}{\sqrt{8}}\{|1\ 2u\ 3\ 4d\rangle - |2\ 1u\ 3\ 4d\rangle - |1\ 2u\ 3\ 4d\rangle - |1\ 2d\ 3\ 4u\rangle + |1\ 2u\ 3\ 4d\rangle + |2\ 1d\ 3\ 4u\rangle + |1\ 2d\ 4\ 3u\rangle - |2\ 1d\ 4\ 3u\rangle\} \quad I_6 = 9$$

$$\Phi_7 = \frac{1}{\sqrt{8}}\{|1\ 2u\ 3\ 4d\rangle + |2\ 1u\ 3\ 4d\rangle - |1\ 2u\ 3\ 4d\rangle + |1\ 2d\ 3\ 4u\rangle - |1\ 2u\ 3\ 4d\rangle + |2\ 1d\ 3\ 4u\rangle - |1\ 2d\ 4\ 3u\rangle - |2\ 1d\ 4\ 3u\rangle\} \quad I_7 = 3$$

$$\Phi_8 = \frac{1}{\sqrt{8}}\{|1\ 2u\ 3\ 4d\rangle + |2\ 1u\ 3\ 4d\rangle - |1\ 2u\ 3\ 4d\rangle - |1\ 2d\ 3\ 4u\rangle - |1\ 2u\ 3\ 4d\rangle - |2\ 1d\ 3\ 4u\rangle + |1\ 2d\ 4\ 3u\rangle + |2\ 1d\ 4\ 3u\rangle\} \quad I_8 = 3 \quad (7)$$

These eight tunneling states lie on the energy levels of the low branch, as shown in Figure 8. The upper eight tunneling states can be constructed in a similar manner, when starting with conformation C', and is not detailed here.

Supporting Information Available: Tables of observed transition lines and vibrational frequencies of TFA monomers and dimers. This material is available free of charge via the Internet at http://pubs.acs.org.

References and Notes

(1) Canagaratna, M.; Phillips, J. A.; Ott, M. E.; Leopold, K. R. *J. Phys. Chem. A* **1998**, *102*, 1489.
(2) Fiacco, D. L.; Hunt, S. W.; Leopold, K. R. *J. Am. Chem. Soc.* **2002**, *124*, 4504.
(3) Priem, D.; Ha, T.-K.; Bauder, A. *J. Chem. Phys.* **2000**, *113*, 169.
(4) McCurdy, P. R.; Hess, W. P.; Xantheas, S. S. *J. Phys. Chem. A* **2002**, *106*, 7628.
(5) Wei, D. Q.; Truchon, J.-F.; Sirois, S.; Salahub, D. *J. Chem. Phys.* **2002**, *116*, 6028.
(6) Chuchev, K.; BelBruno, J. J. *J. Mol. Struct. (THEOCHEM)* **2006**, *763*, 199.
(7) Kisiel, Z.; Białkowska-Jaworska, E.; Pszczółkowski L.; Milet, A.; Struniewicz, C.; Moszynski, R.; Sadlej, J. *J. Chem. Phys.* **2000**, *112*, 5767.
(8) Kisiel, Z.; Pietrewicz, B. A.; Desyatnyk, O.; Pszczółkowski L.; Struniewicz, I.; Sadlej, J. *J. Chem. Phys.* **2003**, *119*, 5907.
(9) Escribano, R.; Couceiro, M.; Gómez, P. C.; Carrasco, E.; Moreno, M. A.; Herrero, V. J. *J. Phys. Chem. A* **2003**, *107*, 651.
(10) Vaida, V.; Headrick, J. E. *J. Phys. Chem. A* **2000**, *104*, 5401.
(11) Scott, B. F.; Spencer, C.; Martin, J. W.; Barra, R.; Bootsma, H. A.; Jones, K. C.; Johnston, A. E.; Muir, D. C. G. *Environ. Sci. Technol.* **2005**, *39*, 8664.
(12) Wallington, T. J.; Hurley, M. D.; Ball, J. C.; Kaiser, E. W. *Environ. Sci. Technol.* **1992**, *26*, 1318.
(13) Møgelberg, T. E.; Nielsen, O. J.; Sehested, J.; Wallington, T. J.; Hurley, M. D. *Chem. Phys. Lett.* **1994**, *226*, 171.
(14) Hurley, M. D.; Sulbaek Andersen, M. P.; Wallington, T. J.; Ellis, D. A.; Martin, J. W.; Mabury, S. A. *J. Phys. Chem. A* **2004**, *108*, 615.
(15) Kotamarthi, V. R.; Rodriguez, J. M.; Ko, M. K. W.; Tromp Sze, N. D. *J. Geophys. Res.* **1998**, *103*, 5747.
(16) Low, R. J.; Varberg, T. D.; Connelly, J. P.; Auty, A. R.; Howard, B. J.; Brown, J. M. *J. Mol. Spectrosc.* **1993**, *161*, 499.
(17) Stolvijk, V. M.; Van Eijck, B. P. *J. Mol. Spectrosc.* **1985**, *113*, 196.
(18) Coudert, L. H.; Hougen, J. T. *J. Mol. Spectrosc.* **1990**, *139*, 259.
(19) Frisch, M. J.; Trucks, G. W.; Schlegel, H. B.; Scuseria, G. E.; Robb, M. A.; Cheeseman, J. R.; Montgomery, J. A., Jr.; Vreven, T.; Kudin, K. N.; Burant, J. C.; Millam, J. M.; Iyengar, S. S.; Tomasi, J.; Barone, V.; Mennucci, B.; Cossi, M.; Scalmani, G.; Rega, N.; Petersson, G. A.; Nakatsuji, H.; Hada, M.; Ehara, M.; Toyota, K.; Fukuda, R.; Hasegawa, J.; Ishida, M.; Nakajima, T.; Honda, Y.; Kitao, O.; Nakai, H.; Klene, M.; Li, X.; Knox, J. E.; Hratchian, H. P.; Cross, J. B.; Bakken, V.; Adamo, C.; Jaramillo, J.; Gomperts, R.; Stratmann, R. E.; Yazyev, O.; Austin, A. J.; Cammi, R.; Pomelli, C.; Ochterski, J. W.; Ayala, P. Y.; Morokuma, K.; Voth, G. A.; Salvador, P.; Dannenberg, J. J.; Zakrzewski, V. G.; Dapprich, S.; Daniels, A. D.; Strain, M. C.; Farkas, O.; Malick, D. K.; Rabuck, A. D.; Raghavachari, K.; Foresman, J. B.; Ortiz, J. V.; Cui, Q.; Baboul, A. G.; Clifford, S.; Cioslowski, J.; Stefanov, B. B.; Liu, G.; Liashenko, A.; Piskorz, P.; Komaromi, I.; Martin, R. L.; Fox, D. J.; Keith, T.; Al-Laham, M. A.; Peng, C. Y.; Nanayakkara, A.; Challacombe, M.; Gill, P. M. W.; Johnson, B.; Chen, W.; Wong, M. W.; Gonzalez, C.; Pople, J. A. *Gaussian 03*, revision C.02; Gaussian, Inc.: Wallingford, CT, 2004.
(20) Møller, C.; Plesset, M. S. *Phys. Rev.* **1934**, *46*, 618.
(21) Boys, S. F.; Bernardi, F. *Mol. Phys.* **1993**, *19*, 553.
(22) Aloisio, S.; Hintze, P. E.; Vaida, V. *J. Phys. Chem. A* **2002**, *106*, 363.

(23) Ziółowski, M.; Grabowski, S. J.; Leszczynski, J. *J. Phys. Chem. A* **2006**, *110*, 6514.
(24) Bunker, P. R.; Jensen, P. *Molecular Symmetry and Spectroscopy*; NRC Research Press: Ottawa, 1998.
(25) Dennison, D. M.; Uhlenbeck, G. E. *Phys. Rev.* **1932**, *41*, 759.
(26) Atkins, P. W. *Physical Chemistry*; Oxford University Press: Oxford, 1994; Chapter 20.
(27) Scott, A. P.; Radom, L. *J. Phys. Chem. A* **1996**, *100*, 16502.
(28) Ellingson, R. G.; Ellis, J.; Fels, S. *J. Geophys. Res.* **1991**, *96*, 8929.
(29) Tao, F. M.; Higgins, K.; Klemperer, W.; Nelson, D. D. *Geophys. Res. Lett.* **1996**, *23*, 1797.
(30) Staikova, M.; Donaldson, D. J. *Phys. Chem. Chem. Phys.* **2001**, *3*, 1999.
(31) Tschumper, G. S.; Leininger, M. L.; Hoffman, B. C.; Valeev, E. F.; Schaefer, H. F., III; Quack, M. *J. Chem. Phys.* **2002**, *116*, 690.